Liquid-Infused Nanostructured Surfaces with Extreme Anti-Ice and Anti-Frost Performance

Philseok Kim,[†,‡] Tak-Sing Wong,[†,‡] Jack Alvarenga,[†] Michael J. Kreder,[†] Wilmer E. Adorno-Martinez,[§] and Joanna Aizenberg[†,‡,⊥,*]

[†]Wyss Institute for Biologically Inspired Engineering and [‡]School of Engineering and Applied Sciences, Harvard University, Cambridge, Massachusetts 02138, United States, [§]Department of Chemistry, College of Natural Sciences, University of Puerto Rico, Rio Piedras, Puerto Rico, and [⊥]Department of Chemistry and Chemical Biology, Harvard University, Cambridge, Massachusetts 02138, United States

ABSTRACT Ice-repellent coatings can have significant impact on global energy savings and improving safety in many infrastructures, transportation, and cooling systems. Recent efforts for developing ice-phobic surfaces have been mostly devoted to utilizing lotus-leaf-inspired superhydrophobic surfaces, yet these surfaces fail in high-humidity conditions due to water condensation and frost formation and even lead to increased ice adhesion due to a large surface area. We report a radically different type of ice-repellent material based on slippery, liquid-infused porous surfaces (SLIPS), where a stable, ultrasmooth, low-hysteresis lubricant overlayer is maintained by infusing a water-immiscible liquid into a nanostructured surface chemically functionalized to have a high affinity to the infiltrated liquid and lock it in place. We develop a direct fabrication method of SLIPS on industrially relevant metals, particularly aluminum, one of the most widely used lightweight structural materials. We demonstrate that SLIPS-coated Al surfaces not only suppress ice/frost accretion by effectively removing condensed moisture but also exhibit at least an order of magnitude lower ice adhesion than state-of-the-art materials. On the basis of a theoretical analysis followed by extensive icing/deicing experiments, we discuss special advantages of SLIPS as ice-repellent surfaces: highly reduced sliding droplet sizes resulting from the extremely low contact angle hysteresis. We show that our surfaces remain essentially frost-free in which any conventional materials accumulate ice. These results indicate that SLIPS is a promising candidate for developing robust anti-icing materials for broad applications, such as refrigeration, aviation, roofs, wires, outdoor signs, railings, and wind turbines.

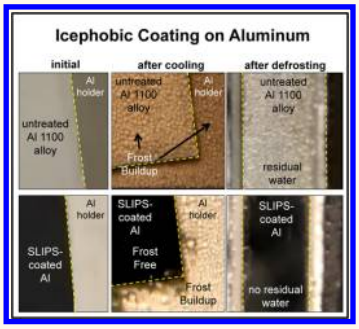

KEYWORDS: anti-frost surfaces · nanostructured coating · slippery liquid-infused porous surface · electrodeposition

Ice formation and accretion present serious economic and safety issues for many essential infrastructures such as aircraft, power lines, wind turbines, marine vessels, and telecommunications equipment, as well as in many commercial and residential refrigerators and freezers.[1−3] Despite the economic significance of having effective ice-repellent materials, state-of-the-art icephobic coatings/surfaces are still far from optimal, as frost and ice can easily build up even under moderate icing conditions (*e.g.*, <−5 °C with relative humidity >50%). During the past decade, progress has been made toward understanding the use of lotus-leaf-inspired superhydrophobic surfaces for the prevention of ice formation.[1−11] Under a frost-free environment (*e.g.*, low humidity conditions), superhydrophobic surfaces show promising behavior in preventing ice formation[2,10,11] even at temperatures as low as −25 to −30 °C.[2] However, recent studies have shown that lotus-leaf-inspired surfaces, due to their high surface area and increased nucleation site density to condensing droplets, may induce ice nucleation at an even faster rate than smooth surfaces of the equivalent materials at high-humidity conditions.[7,12] As a result, frost can build up within the complex topographical features of superhydrophobic surfaces, making their ice adhesion significantly stronger than that of smooth surfaces and substantially increasing the amount of energy required to remove the accumulated ice.[3−5]

Current knowledge on icephobic materials suggests that creating a surface with a low contact angle hysteresis (defined as the difference between the advancing and receding contact angles) can significantly reduce the ice adhesion, which is typically achieved by introducing highly textured surfaces to decrease the ice-contacting area.[1,4,9] Alternatively, creating an *extremely smooth surface* with low wettability could be another strategy for reducing contact angle hysteresis and delaying frost formation while also reducing ice adhesion, especially in high-humidity conditions.[12] However, the inherent limits on surface

* Address correspondence to jaiz@seas.harvard.edu.

Received for review May 24, 2012 and accepted June 10, 2012.

Published online June 10, 2012
10.1021/nn302310q

energy reduction, combined with the lack of any practical way to eliminate the intrinsic defects and inhomogeneities that contribute to liquid pinning, freezing, and ice adhesion, have raised the question of whether any solid surface can ever be truly ice-preventive.

Herein we report a radically different type of ice-repellent materials that present a dynamic, molecularly smooth *liquid* interface capable of repelling condensing water droplets and showing dramatic reduction in ice adhesion and droplet retention size compared to the state-of-the-art materials.[4,5] The approach is based on our recently reported pitcher plant-inspired slippery surfaces,[13] which are created by infiltrating a micro/nanoporous substrate with a lubricating liquid to produce a thin, ultrasmooth lubricating layer that repels almost any immiscible materials. We show how slippery, liquid-infused porous surfaces (SLIPS) can be directly fabricated on industrially relevant metals, particularly aluminum, one of the most widely used lightweight structural materials for aircraft, refrigeration, and construction industries. We demonstrate that SLIPS-coated Al surfaces not only suppress ice/frost accretion by effectively removing condensed moisture even in high-humidity conditions but also exhibit at least an order of magnitude lower ice adhesion than state-of-the-art materials.[4]

RESULTS AND DISCUSSION

To create ice- and frost-repellent surfaces, we utilize the principle of minimization of contact angle hysteresis (*i.e.*, the difference between the advancing and receding contact angles)—an approach different from exploring high contact angle, mixed-boundary surfaces in superhydrophobic materials. Since pinning of a liquid to the exposed surface defects is the main reason for high hysteresis and therefore for the formation of immobilized water droplets and their subsequent freezing on cooled solid substrates, our ultralow hysteresis SLIPS surfaces are designed to expose a defect-free, molecularly flat liquid interface. The key to achieving this property is to create a lubricating film that overcoats the solid support which functions to stabilize and hold the lubricant in place. As a result, water droplets that condense on such an interface have minimal exposure to the underlying solid defect sites and are capable of sliding off the surface at very low tilt angles.

SLIPS is designed based on three important criteria: (I) the lubricating fluid and the repellent fluid have to be immiscible; (II) the chemical affinity between the lubricating fluid and the solid should be higher than that between the repellent fluid and the solid; and (III) the solid surface should preferably have roughened nanostructures to provide increased surface area for the adhesion and the retention of the infiltrated lubricating fluid.[13] While we have shown that SLIPS satisfying these conditions can be made on polymeric surfaces, of practical importance is the ability to create such nanostructured coatings on metals. Particularly significant for anti-icing technologies is the development of ice- and frost-free aluminum surfaces, as Al is one of the most widely used metals as cooling fins in heat exchangers and lightweight structural materials for aircrafts, marine vessels, and in the construction industry. Here we develop an Al-based material that satisfies SLIPS criteria by electrodeposition of highly textured polypyrrole (PPy) on Al substrates followed by fluorination of the structured coating and infiltration with the lubricant.

We adapt and optimize our recently developed protocol for modifying the structure of gold-coated surfaces[14,15] to be applicable for the deposition of a nanostructured PPy overcoating on aluminum. Electrodeposition of PPy provides fine control of the morphology at the nanometer scale, achieved by varying the concentration of the monomer, the applied potential, and the deposition time. In addition, we chose this method of creating nanostructured overcoating on aluminum because (I) it can be applied to arbitrarily shaped metallic surfaces; (II) the coating can be applied over a large area; (III) PPy is a good anticorrosive coating material; (IV) the coating can be done at low temperature and does not require any high-temperature annealing or drying process; (V) the method uses aqueous solutions that do not generate toxic chemical waste.

As schematically shown in Figure 1a, we used cooling fins made of extruded sheets of industrial grade pure aluminum (alloy 1100) removed from a heat exchanger as the working electrode (WE) in the standard three-electrode configuration for the oxidative electrochemical deposition of PPy, with sodium dodecylbenzene sulfonate (Na^+DBS^- or SDBS) as a surfactant and counteranion (DBS^-) to compensate for the positive charges produced after the oxidative polymerization. A constant voltage of 0.85 V *vs* a Ag/AgCl reference electrode (RE) was applied for 5−10 min, during which the surface of aluminum gradually became dark blue to black in color (Figure 1b). Figure 2a,b shows typical linear scanning voltammetry and chronoamperometry curves during the deposition. The PPy was predominantly deposited on the surface facing the platinum mesh counter electrode (CE) and resulted in uniform PPy films of *ca.* 3−4 μm thickness. We confirmed the scalability of our method by performing electrodeposition of PPy over a large area sample, up to 10 cm × 10 cm (SFigure 1 in Supporting Information). Therefore, further scale-up and application of our method to any arbitrarily shaped Al surface should be straightforward as the electrodeposition can be simply performed in a large bath using a voltage rectifier or even using a battery. We also performed cyclic voltammetry for the PPy coating on aluminum

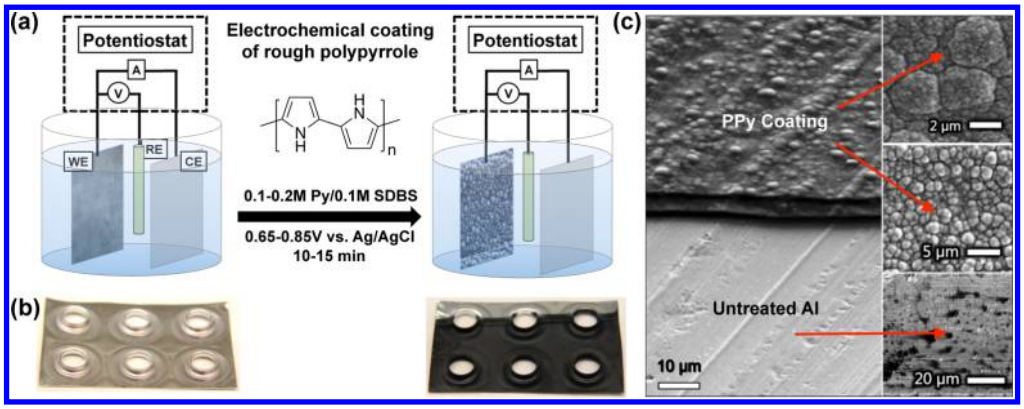

Figure 1. (a) Schematics of the procedure for electrochemical coating of nanostructured polypyrrole on aluminum sheet (WE, Al 1100 alloy as working electrode; RE, Ag/AgCl reference electrode; CE, Pt gauze counter electrode). (b) Photographs of untreated punch-pressed aluminum sample (left) and partially coated aluminum sample (right). PPy-coated area appears black in the picture. Substrate size = 6 cm × 9 cm. (c) SEM images comparing the morphology of untreated area of aluminum with PPy-coated area. Insets show higher magnification SEM images for the two areas.

and observed the reversibility of the reduction/oxidation (Figure 2c) that confirms the incorporation of the dopant ions. Importantly, the dopant−monomer arrangement in the polymer chain and the templating effect due to micelle formation above the critical micelle concentration of SDBS are responsible for specific structural features of the deposited film.[16,17]

Figure 1c compares the topographies of the resultant PPy/Al surfaces and untreated Al. As seen in SEM images, the PPy coating shows the rough and globular morphology of the PPy layer, with diameters ranging from submicrometer up to ~2 μm. Higher magnification SEM images further revealed the hierarchical nature of the surface coating, in which each large globule consists of smaller nanoscale bumps providing increased surface area for lubricant infiltration and retention. To form SLIPS, the PPy-coated aluminum samples were fluorinated with (tridecafluoro-1,1,2,2-tetrahydrooctyl)trichlorosilane and infiltrated with a low-viscosity perfluorinated lubricating fluid (Krytox 100, DuPont).[13] While high-viscosity coatings ("anti-icing" non-Newtonian fluid) have been primarily used for anti-icing purpose on smooth metal surfaces in aviation due to longer holdover time than that of low-viscosity coatings ("de-icing" Newtonian fluid) that are applied at high temperature (71−82 °C) and pressure in order to deice the aircraft before application of the high-viscosity anti-icing fluid, these high-viscosity, non-Newtonian, fluid-based coatings require extremely high shear force to create a thin liquid coating with low ice adhesion to prevent the contaminants (*e.g.*, ice, snow) from adhering to the aircraft surface.[18] However, for many other anti-icing applications where gravity and light vibration are the only sources of shear force, a low-viscosity Newtonian fluid (7 cSt at 20 °C for Krytox 100) presents a much better choice to effectively create SLIPS with its smooth and thin liquid interface locked in the nanostructured solid. In addition, our choice of a low-viscosity perfluorinated lubricant is also due to its immiscibility with water, low freezing point (<−70 °C), and strong chemical affinity to fluoro-silanized solid substrate, which are important criteria to form SLIPS at low temperatures.

To characterize SLIPS-coated Al (SLIPS-Al) as an icephobic material, we investigated the contact angle hysteresis, water droplet retention behavior, frost formation process, and the ice adhesion characteristics of aluminum samples with various surface treatments. In general, in a humid and cold environment, a condensed water droplet formed on an inclined, cold surface will initially be pinned due to the surface heterogeneity. With continued condensation, the basal diameter of the sliding droplet, which has the shape of a spherical cap, increases until it reaches a critical value, D_c, above which the droplet will slide along the surface. The retention of the droplet is dictated by two competing forces: gravity and the surface tension acting along the contact line of the droplet (*i.e.*, the surface retention force). Quantitatively, the critical diameter of the droplet can be estimated from an equilibrium where these two forces counteract each other, which can be further elaborated as[19]

$$\rho V g \sin\alpha = \gamma D_c(\cos\theta_R - \cos\theta_A) \quad (1)$$

where ρ is the density of water, V is the volume of the droplet, g is the standard acceleration due to gravity, α is the tilting angle, γ is the surface tension of water, θ_R is the receding contact angle, and θ_A is the advancing contact angle.

It is important to note that surface retention force is a strong function of the contact angle hysteresis (CAH, $\Delta\theta = \theta_A - \theta_R$). Therefore, one can minimize the critical size of the water droplets retained on the surface by minimizing CAH. Practically, this ensures efficient removal of condensed water droplets by enabling them to slide off the surface before they can freeze. We have measured the advancing and receding contact angles of a macroscopic water droplet (*i.e.*, ~5 μL) for

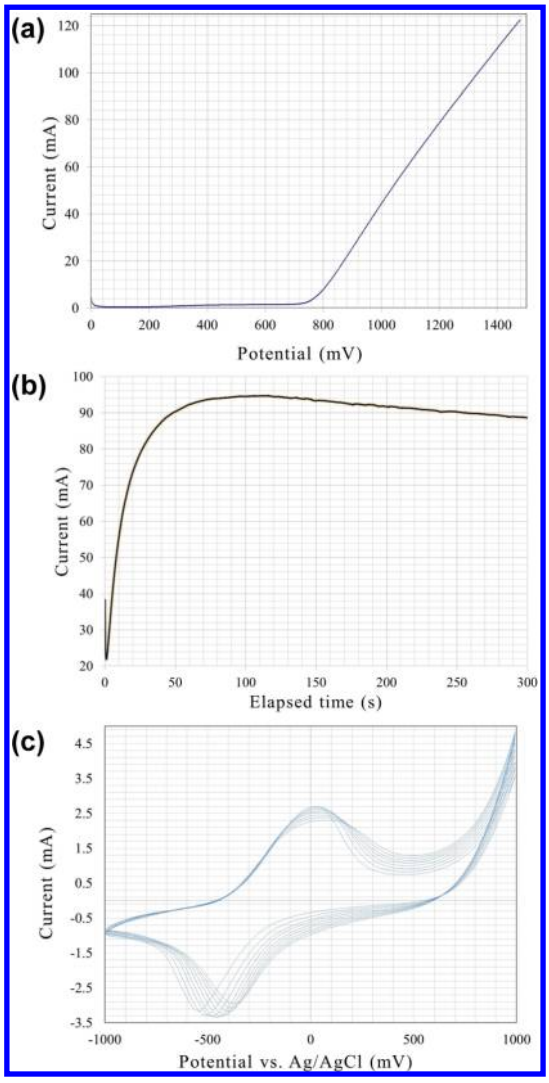

Figure 2. (a) Linear scan voltammogram (LSV) recorded from a voltage sweep from 0 to 1.5 V with a scan rate of 0.01 V/s in the PPy coating solution using aluminum 1100 as the working electrode. The onset of the polypyrrole growth was observed at about 0.75 V as indicated by the increase of the Faradaic current which continued to increase linearly. This LSV experiment allows us to define the lowest possible applied voltage range to polymerize pyrrole. On the basis of this curve, we chose 0.85 V as the electrodeposition potential. (b) Typical chronoamperogram (current *vs* time) recorded during the PPy coating process. The dimension of the substrate is about 3 cm × 8 cm (average current density is ~3.8 mA/cm^2). The current density was varied for different substrate sizes. For example, for 8 cm × 8 cm substrates, the current density was kept at about 1.9 mA/cm^2 for the best result. (c) Cyclic voltammetry of the PPy coating on aluminum substrate in 0.1 M SDBS solution. The potential of the initial 75 s was swept at 0.1 V/s, between −0.85 V and +0.5 V.

untreated aluminum alloy 1100 (Al), Krytox 100-coated aluminum (K100-Al), hydrophobically modified aluminum (F13-Al), Krytox 100-coated hydrophobic aluminum (K100-F13-Al), superhydrophobic PPy-coated aluminum (F13-PPy-Al), and for SLIPS-Al (K100-F13-PPy-Al) at room temperature to determine the CAH, which is summarized in Table 1. Our measurements indicated that the CAH of SLIPS-Al ($\Delta\theta = 2 \pm 1°$) was

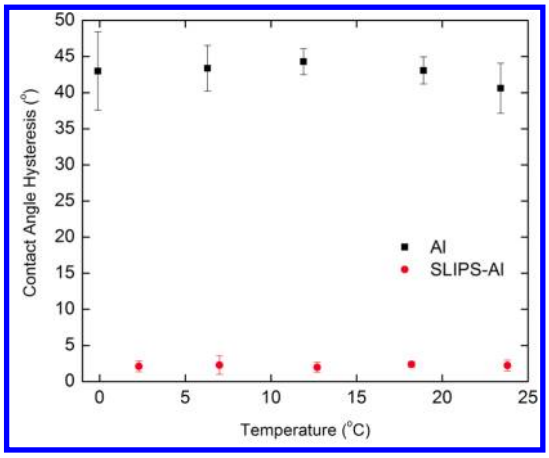

Figure 3. Contact angle hysteresis (CAH) of water on bare aluminum (Al) and SLIPS-Al measured at different temperatures. Error bars represent standard derivations for at least five independent measurements.

considerably smaller than that of the untreated Al ($\Delta\theta = 41 \pm 4°$) and Al samples with other surface treatments, and that the CAH did not change significantly with temperature, as shown in Figure 3. Given the large CAH of the bare Al and other surface-treated Al samples, this further illustrates that conventional materials are inefficient in removing water condensates by gravitational force alone. To obtain the critical diameter of the droplet, D_c, one can express the droplet volume as a function of θ_A and rearrange eq 1 as[19]

$$D_c = \left(\frac{24\sin^3\theta_A\gamma(\cos\theta_R - \cos\theta_A)}{\pi\rho(1-\cos\theta_A)^2(2+\cos\theta_A)g\sin\alpha} \right)^{1/2} \quad (2)$$

By incorporating the data from Table 1 into eq 2, we estimated that the critical droplet diameter is about 8 times smaller for SLIPS-Al (~600 μm at $\alpha = 90°$ and ~1.5 mm at $\alpha = 10°$) than for bare aluminum (~5.0 mm at $\alpha = 90°$ and ~12.0 mm at $\alpha = 10°$) at room temperature (Figure 4).

We have experimentally verified these estimates by observing the behavior and sliding probability of manually dispensed water droplets on inclined SLIPS-Al and various surface modified Al samples at room temperature. In Figure 4, these data are plotted to show the critical droplet size below which droplets will remain pinned to the surface (area above each curve). For the area below the curves, droplets will slide due to gravity and be removed from the substrate. It is important to note that the droplets retained on the SLIPS-Al are about 8 times smaller in diameter (~500 times smaller in volume) at each tilt angle examined than those retained on the bare Al surface. For example, at a tilt angle of 90°, all droplets larger than ~600 μm slide on SLIPS-Al surface whereas only droplets larger than ~5 mm slide on the bare aluminum surface. The results verified that conventional approaches of using hydrophobic or superhydrophobic Al slightly improve the efficiency of

TABLE 1. Advancing and Receding Contact Angles, Contact Angle Hystereses, and Ice Adhesion Strengths of Various Aluminum Surfaces Tested (All Reported Values Are Average Values from Five or More Independent Measurements)

sample type	sample name	advancing contact angle[a] (deg)	receding contact angle[a] (deg)	contact angle hysteresis[a] (deg)	ice adhesion strength (at −10 °C) (kPa)
roughness (−) affinity (−) lubricant (−)	Al	46 ± 5	6 ± 2	41 ± 4	1360 ± 210
roughness (−) affinity (−) lubricant (+)	K100-Al	75 ± 8	7 ± 2	68 ± 7	1070 ± 150
roughness (−) affinity (+) lubricant (−)	F13-Al	107 ± 3	30 ± 4	77 ± 2	1145 ± 310
roughness (−) affinity (+) lubricant (+)	K100-F13-Al	118 ± 5	41 ± 10	78 ± 12	515 ± 130
roughness (+) affinity (+) lubricant (−)	F13-PPy-Al	143 ± 4	62 ± 1	81 ± 4	845 ± 52
roughness (+) affinity (+) lubricant (+)	K100-F13-PPy-Al (SLIPS-Al)	117 ± 3	115 ± 3	2 ± 1	15.6 ± 3.6

[a] Indicates measurements at room temperature.

removing water droplets compared to hydrophilic surfaces.[20] However, lubricating Al samples that lack either surface roughness or proper surface chemistry did not noticeably improve the droplet sliding behavior, due to their inability to retain a stable lubricant layer. Overall, SLIPS-Al is capable of removing water condensates much more effectively than the conventional materials.

To test the advantages of this behavior at freezing conditions, and to understand the process of frost formation on the SLIPS-Al surfaces, we built a custom humidity-controlled chamber in which all of the frosting/defrosting experiments that simulated refrigeration conditions were carried out in 60% relative humidity (RH). We used a thermoelectric or liquid-nitrogen-cooled cold stage to precisely control the temperature of the aluminum substrates. Figure 5 compares snapshots of a SLIPS-Al and a bare Al surface at room temperature prior to testing, during a cooling cycle, after a deep freezing, and during a defrost cycle. As shown in Figure 5 and movies 1 and 2 in the Supporting Information, water condenses on both surfaces at high humidity. Growth of each condensate droplet, as well as the coalescence of droplets, led to an overall gradual increase of the droplet size over time. Significantly, even under a very rapid cooling rate, 2 °C/min, the droplets formed on SLIPS-Al grew beyond the critical droplet size for the tilt angle tested (75°) and were able to slide down and leave the SLIPS-Al surface before freezing, whereas all of the droplets on untreated aluminum could not exceed the larger critical droplet size on these surfaces and froze before they could slide. We expect that this droplet growth and sliding behavior on SLIPS-Al will become a much more significant factor in reducing the total accumulation of ice under real refrigeration conditions, where the cooling rate should be much less than 2 °C/min (typically 3−5 °C/h). After a prolonged exposure to deep freezing (*e.g.*, <−10 °C) and high-humidity conditions (60% RH), SLIPS-Al surfaces eventually accumulate ice, although still mostly growing from the edges connected to other non-SLIPS surfaces, as shown in Figure 5.

It is noteworthy that the morphology of the ice formed on SLIPS-Al was significantly different from that on bare Al, primarily due to the difference in the contact angle as similarly observed on other lotus-leaf-inspired superhydrophobic surfaces.[2] In addition, since some of the large sliding supercooled water droplets can freeze upon finding a nucleation site on the surface during sliding, ice tends to occur in large and isolated patches on SLIPS-Al. During the defrost cycle, these large ice patches slide off the surface immediately upon melting at the interface with the SLIPS-Al, leaving the surface clean and ready for the next cooling cycle almost instantaneously (∼1 min). In contrast, the ice accretions on bare aluminum tend to have a densely packed sheet morphology that is hard to remove in a defrost cycle. Moreover, even when most of the ice melted, the surface of bare Al was covered with firmly pinned droplets. These droplets were retained on the surface and could only be removed by full evaporation that occurred at elevated temperature (∼25 °C) after >20 min. These results indicate that SLIPS-Al not only delays the frost formation as compared to bare Al but also accelerates the removal of frost using a much reduced energy input owing to the small surface retention forces.

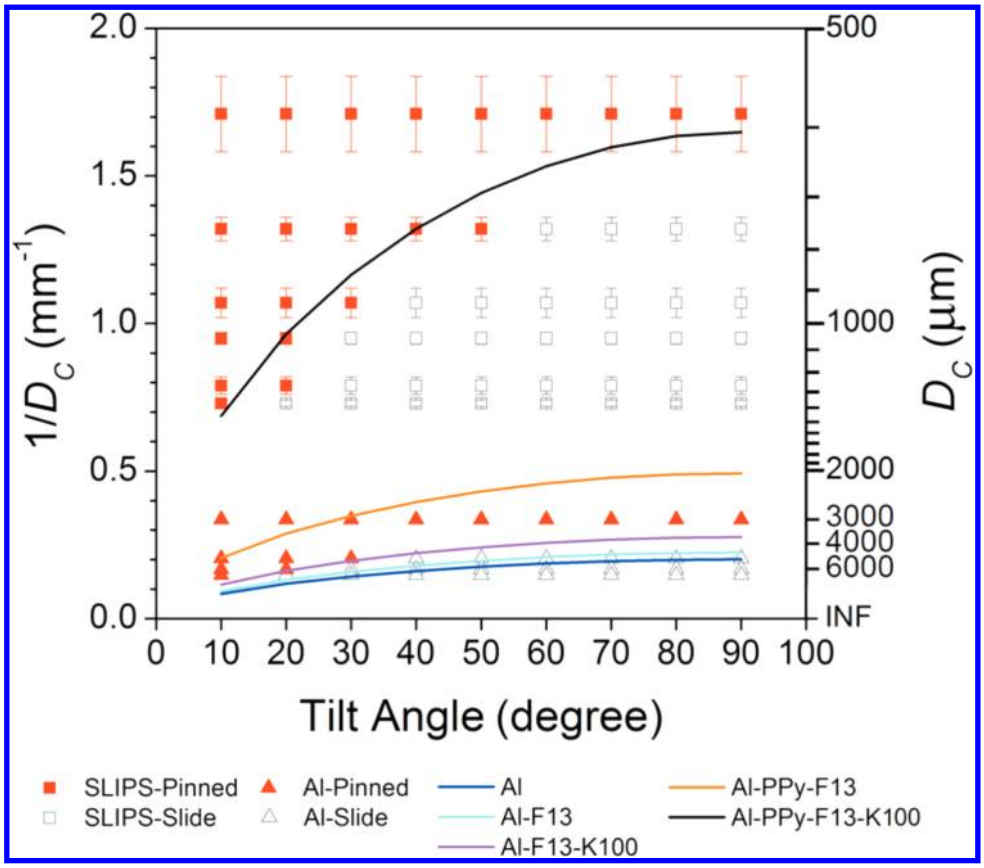

Figure 4. Droplet retention phase diagram for various aluminum surfaces tested. The inverse of the critical droplet size (D_c) at each given tilt angle is plotted. The lines indicate theoretical boundaries (eq 2) for droplets pinning and sliding on each of the aluminum surfaces. The water droplets smaller than the critical droplet size corresponding to the area above each curve will remain pinned, while the water droplets larger than the critical droplet size corresponding to the area below each curve will slide and be removed from the substrate. Experimental results for Al (triangles) and SLIPS-Al (squares) taken at various droplet sizes and tilt angles are overlaid on these theoretical boundaries. Open and filled triangles and squares represent data for sliding and pinned droplets, respectively. For each given droplet size and tilt angle, we defined the droplet as "sliding" if more than 8 out of 10 applied droplets were sliding. Error bars indicate the uncertainty in the droplet size measurement.

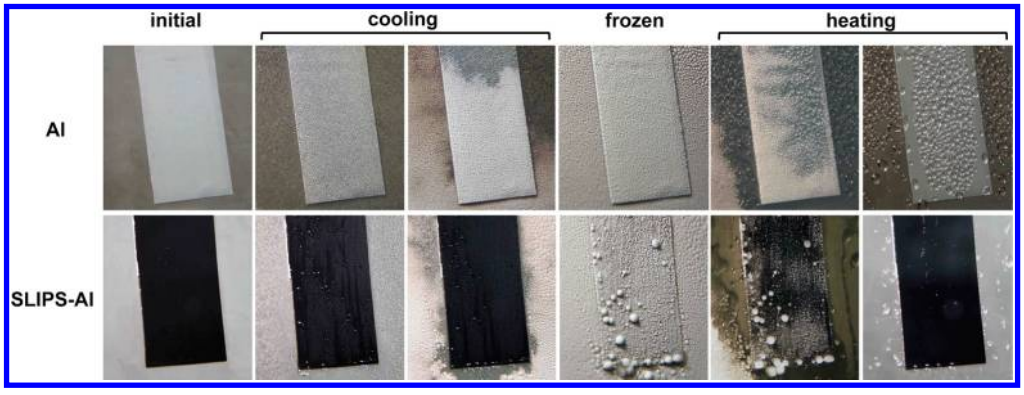

Figure 5. Still images extracted from the movies simulating ice formation by deep freezing (−10 °C) in high-humidity condition (60% RH) and subsequent deicing by heating (see representative movies 1 and 2 in the Supporting Information). The morphology of accumulated ice on SLIPS-Al is significantly different from that on bare Al. Condensation/freezing cycle: from room temperature to −10 °C at 5 °C/min. Melting (defrost) cycle: from −10 to 25 °C at ~10 °C/min. Ice still forms mostly around the edges of SLIPS-Al by bridging from the surrounding aluminum substrate, while it forms uniformly all over the aluminum substrate. Several defects (tall features above the level of the lubricant layer) on the surface of SLIPS-Al led to the pinning of droplets while they were sliding which eventually led to the formation of large ice crystals on SLIPS-Al. The samples are mounted with 75° tilt angle, and the widths of the substrates are approximately 3 cm.

We also tested various large Al surfaces (10.5 cm × 10.5 cm) under a prolonged exposure to freezing temperatures slightly below 0 °C (*e.g.*, −2 °C) and high-humidity conditions (60% RH) (Figure 6). Even under this condition, all other Al surfaces were quickly covered with ice, while essentially a frost-free surface

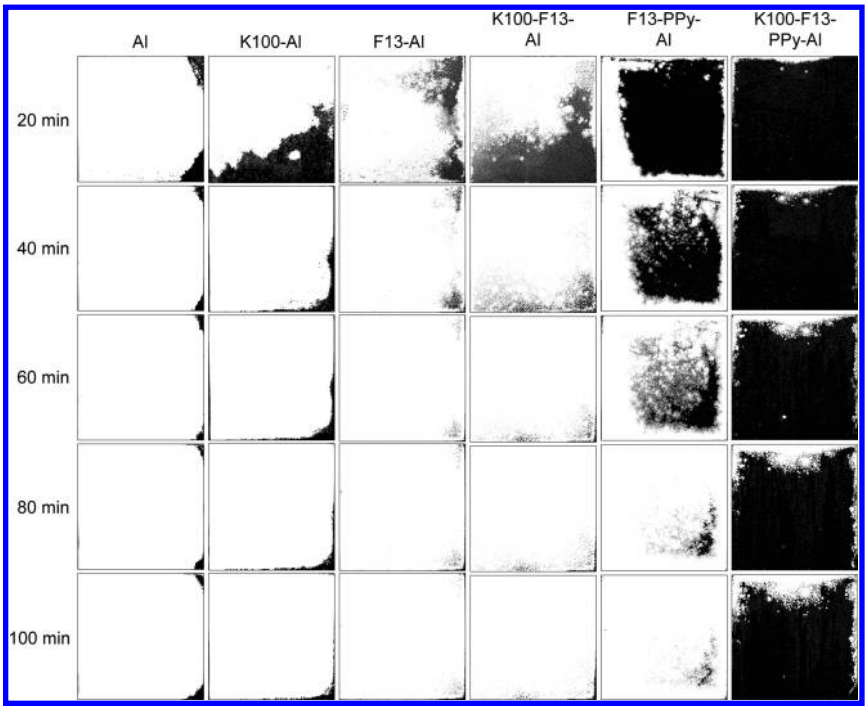

Figure 6. Time lapse images of ice formation experiments at −2 °C in high-humidity conditions (60% RH) on various aluminum surfaces tested (see movie 3 in the Supporting Information comparing K100-F13-Al and SLIPS-Al). Digital pictures were converted to a 16-bit grayscale images and thresholded using ImageJ to accurately reflect ice-covered areas (white) and uncovered areas (black). After 20 min of freezing, >∼90% of bare aluminum (Al) and greased aluminum (K100-Al) surfaces are covered with ice. After 40 min of freezing, >∼95% of all aluminum sample surfaces are covered with ice except for superhydrophobic (F13-PPy-Al) and SLIPS (K100-F13-PPy-Al) coated aluminum samples. After 100 min of freezing, >∼99% of all aluminum surfaces are covered with ice while only ∼20% of SLIPS-Al surface is covered with ice. Although some ice formation is observed on SLIPS-Al, these are mainly due to the edge effect especially around the inlet of the coolant (liquid nitrogen) on the top edge of the cold plate used and the bulk of SLIPS-Al remains ice-free. The substrates are mounted vertically and are approximately 10.5 cm × 10.5 cm in size. See also Figure 7 for the characterization of the surface area covered by ice as a function of cooling time.

was maintained on the bulk area of SLIPS-Al for at least 100 min, except for the edges where the ice grew only by bridging from the surrounding non-SLIPS surface connected to the SLIPS-Al and around the inlet of the liquid nitrogen coolant (top edge) where the local temperature can fluctuate much below −2 °C during the active feedback control of the temperature. Movie 3 compares cooling and heating cycles of lubricated hydrophobic Al (K100-F13-Al) and SLIPS-Al (K100-F13-PPy-Al). Figure 7 compares the fractions of the surface covered by ice on the aluminum samples shown in Figure 6 as a function of cooling time. The increase in the surface coverage by ice on the SLIPS-Al sample (K100-F13-PPy-Al) is mostly due to the edge effect. It should be noted that the heating cycle for SLIPS-Al was implemented after continuous cooling for 5 h, at which time the surface coverage of ice (∼64%) was still less than any of the other substrates after 100 min.

We have further evaluated the ice adhesion strength of SLIPS-Al and Al surfaces using a custom ice adhesion test setup based on the methods described previously (SFigure 2, movies 4 and 5).[4,15] Briefly, we formed ice in fluoroalkyl-silanized glass columns with contact areas of approximately 24 mm^2 on a surface-treated Al substrate and pulled or pushed the samples at a constant rate to determine the ice adhesion force as the maximum force prior to adhesive failure. None of our samples suffered from cohesive failure of the ice itself. The average ice adhesion strength on SLIPS-Al was close to the limit of the gauge used and measured to be 15.6 kPa, which is 2 orders of magnitude lower than that on bare Al (1359 kPa) and an order of magnitude lower than that on the state-of-the-art icephobic materials (165 kPa).[4] We attribute such low ice adhesion strength to the ultrasmooth solid−liquid interface present at the SLIPS surface, which has significantly fewer defects/heterogeneities/pinning points than the solid−solid interface found in superhydrophobic surfaces.

Clearly, such characteristics as highly reduced sliding droplet sizes, delayed frost formation, and ultralow adhesion strength make the SLIPS-Al a promising candidate for developing robust anti-icing materials. Unlike lotus-leaf-inspired icephobic surfaces, which fail under high-humidity conditions, SLIPS-based icephobic materials, as our results suggest, can completely prevent ice formation at temperatures slightly below 0 °C, while dramatically reducing ice adhesion under deep freezing, frost-forming conditions. The latter

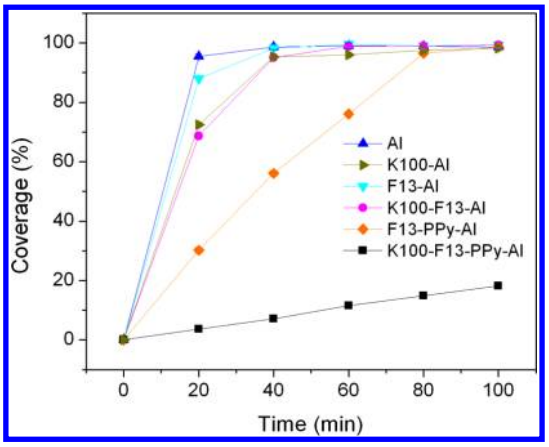

Figure 7. Fraction of the surface covered by ice on large aluminum samples (10.5 cm × 10.5 cm) shown in Figure 6 as a function of cooling time at −2 °C and at 60% RH. The increase in the surface coverage on the SLIPS-Al sample (K100-F13-PPy-Al) is mostly due to edge effect.

facilitates the efficient removal of ice and lowers energy costs associated with it. In particular, we show that the full defrosting of SLIPS-coated Al occurs in ∼1 min at temperatures only slightly above the melting temperature (∼5 °C). As a comparison, modern "frost-free" or "auto-defrost" cooling systems use a built-in heating element to remove frost formed on the surface of the heat exchanger by raising the temperature to ∼25 °C. Such a procedure is typically repeated up to six times a day with 15−30 min of active heating during each defrost cycle, which imposes a significant amount of energy consumption.

CONCLUSIONS

We have demonstrated a scalable and reproducible coating method to create a slippery, icephobic surface on industrially relevant material, specifically aluminum. We have shown that SLIPS-coated aluminum surfaces not only significantly reduce ice accumulation by allowing the condensed water droplets to slide off before they freeze but also enable the easy removal of the accumulated ice and melted water by gravity at low tilt angles. The 1−2 orders of magnitude reduced ice adhesion strength of SLIPS (∼15 kPa on SLIPS-Al) compared to conventional materials presents a great opportunity to utilize SLIPS-based icephobic surfaces for broad applications in the refrigeration and aviation industry, as well as in other high-humidity environments when an icephobic surface is desirable, such as roofs, wires, outdoor signs, railings, and wind turbines, where ice can be easily removed by tilting, agitation (*e.g.*, wind or vibrations), or even by a weak shear force.

EXPERIMENTAL SECTION

Al Sample Preparation and Coating. Aluminum fins from a refrigerator heat exchanger assembly and rolls of extruded aluminum sheet (aluminum alloy 1100) were provided by Luvata, LLC. The raw material was cut into equally sized samples, which were then flattened using a hydraulic press. The aluminum sheets were cleaned by sonication in acetone for 15 min and dried under a stream of nitrogen. Hydrophobic aluminum (F13-Al) samples were prepared by vapor priming (tridecafluoro-1,1,2,2-tetrahydrooctyl)trichlorosilane (Gelest) for 48 h under vacuum. We used a previously reported method for electrodeposition of polypyrrole (PPy).[14,15] Briefly, 0.1−0.2 M pyrrole (Py) solution was prepared using 0.1 M sodium dodecylbenzene sulfonate (SDBS) aqueous solution as a solvent. In this solution, aluminum sheets served as the working electrode and a platinum gauze was used as a counter electrode. Polypyrrole was potentiostatically deposited (+0.85 V *vs* Ag/AgCl) for 300−900 s. After the electropolymerization, the coated samples were rinsed with DI water and dried under a stream of nitrogen.

Characterization of Surface Coating. Scanning electron micrographs (SEMs) were recorded for all representative samples prepared without additional conductive coating, using a thermionic SEM (JSEM-6390LV, JEOL) and a field emission SEM (Ultra 55, Zeiss). The thickness of the PPy coating was measured using a stylus profilometer (Dektak 6M, Veeco). We performed cyclic voltammetry on a freshly prepared PPy film on aluminum in 0.1 M SDBS solution by sweeping the voltage from −1.0 V to +1.0 V at 10 mV/s.

Formation of SLIPS. The PPy-coated aluminum samples were placed in a desiccator with (tridecafluoro-1,1,2,2-tetrahydrooctyl)trichlorosilane (Gelest) for 48 h under vacuum to render the surfaces hydrophobic. We then covered the hydrophobized PPy-coated aluminum samples by applying droplets of a perfluorinated lubricant, perfluoroalkylether (Krytox 100, immiscible with most polar and nonpolar liquids; chemically stable; wide operation temperature range, very low freezing point (<−70 °C), DuPont), then stood the samples vertically to remove excess lubricant until no macroscopic movement of lubricant on the surface was evident. Lubricated aluminum surfaces (K100-Al and K100-F13-Al) were also prepared using the same method. We estimated the thickness of the lubricating layer to be 8−10 μm based on the measured weight change, substrate size, and the density of the lubricating liquid.

Contact Angle Hysteresis and Critical Droplet Size Measurements. The contact angles of DI water were measured using a contact angle goniometer (CAM 101, KSV Instruments) at room temperature. We used five independent measurements to calculate the average advancing and receding contact angle. The surface tension of water was measured based on the pendant drop method. The critical droplet sizes at a given tilt angle were determined by fixing the substrates onto an adjustable tilt stage and testing for droplet mobility, which consisted of dispensing a series of 10 equal volume droplets of deionized water onto different areas on the tilted sample surface. For SLIPS-Al testing, the volume of droplets ranged from 0.25 to 1.50 μL, whereas bare Al required testing with much larger droplets of 7, 40, 60, and 80 μL. If at least 8 out of the 10 dispensed droplets slid down the surface at a given angle, we recognized the conditions as favorable to droplet shedding. We measured the basal diameters for the corresponding droplet volumes independently, prior to tilting experiments, with a digital optical microscope.

Icing and Deicing Tests. A custom humidity and temperature-controlled chamber was built and used for all the ice/frost formation tests. The samples were mounted on the flat aluminum plate of a thermoelectric temperature controller (mK 1000 or STC200, Instec) using either thermally conductive tape or paste. The humidity was actively controlled to maintain a constant relative humidity (RH). After reaching a steady RH of 60%, the temperature of the samples was set to either room temperature or 5 °C. From this point, we recorded videos while cooling the samples to either −2 or −10 °C at 2 °C/min. We also recorded the defrosting process while heating the thermoelectric temperature controller to 5 °C at

5 °C/min. We used an infrared camera (SC5000, FLIR) to confirm the uniformity of the temperature for the thermoelectric temperature controller and a digital SLR (EOS 60D, Canon) for recording the videos. To check the edge effect on a small sample, we fabricated a large area SLIPS-Al sample (10.5 cm × 10.5 cm) and tested it under a frost-forming condition (−2 °C, 60% RH, kept for 100 min for all other Al samples; kept for 5 h for SLIPS-Al sample) to locate the initiation point for the frost build-up on the SLIPS-Al surface.

Ice Adhesion Strength Measurement. We performed all ice adhesion measurements within the humidity-controlled chamber used for the frost and defrost testing. Cylindrical glass columns were made by cutting Pasteur pipettes with a well-polished end. To hydrophobize the glass, we treated it with oxygen plasma for 180 s and placed it under vacuum in a desiccator with (tridecafluoro-1,1,2,2-tetrahydrooctyl)trichlorosilane for at least 24 h. We attached SLIPS-Al and bare Al to a temperature-controlled aluminum plate using thermally conductive tape, placed the glass columns on the substrate, and filled them with 150 μL of fresh deionized water (Millipore Milli-Q A10). Each column had a contact area with the substrate of approximately 24 mm^2. We then decreased the humidity below 3% RH in order to avoid frost formation. We lowered the temperature of the substrate at a rate of 2 °C/min until ice formed, generally at a substrate temperature of −20 °C or below to ensure freezing.[21] After ice formation occurred, we raised the temperature to −10 °C at a rate of 2 °C/min and allowed the samples to equilibrate for a minimum of 30 min. We measured the applied force while maintaining this temperature using a Wagner Instruments Force One FDIX with a maximum force of 50 N and an accuracy of ±0.25 N. A custom force gauge attachment was used to apply force by either pulling or pushing the sample columns at a contact point less than 1 mm above the surface of the substrate. We mounted the force gauge on a syringe pump (Harvard Apparatus PhD Ultra) that was moved forward and backward at a precise rate: 0.5 mm/s for bare Al and all other surface-treated Al samples and 0.1 mm/s for SLIPS-Al due to the large difference in the ice adhesion.

Conflict of Interest: The authors declare no competing financial interest.

Acknowledgment. This research was supported by the MRSEC under NSF Award #DMR-1005022. Part of this work was performed at the Center for Nanoscale Systems (CNS) at Harvard University, supported under NSF Award #ECS-0335765. T.S.W. would like to thank the Croucher Foundation Postdoctoral Fellowship. W.A.M. would like to thank REU BRIDGE, cofunded by the ASSURE program of the DoD in partnership with the NSF REU Site program under NSF Grant #DMR-1005022. We thank Dr. Mike Heidenreich (Luvata, LLC) for kindly providing aluminum samples. We thank Tom Blough for technical assistance in building ice adhesion test setup, Drs. Michael Aizenberg, Alison Grinthal, and Mughees Khan for their comments in manuscript preparation.

Supporting Information Available: Additional figures and movie descriptions. This material is available free of charge *via* the Internet at http://pubs.acs.org.

REFERENCES AND NOTES

1. Yao, X.; Song, Y.; Jiang, L. Applications of Bio-Inspired Special Wettable Surfaces. *Adv. Mater.* **2011**, *23*, 719.
2. Mishchenko, L.; Hatton, B.; Bahadur, V.; Taylor, J. A.; Krupenkin, T.; Aizenberg, J. Design of Ice-Free Nanostructured Surfaces Based on Repulsion of Impacting Water Droplets. *ACS Nano* **2010**, *4*, 7699–7707.
3. Meuler, A. J.; McKinley, G. H.; Cohen, R. E. Exploiting Topographical Texture To Impart Icephobicity. *ACS Nano* **2010**, *4*, 7048–7052.
4. Meuler, A. J.; Smith, J. D.; Varanasi, K. K.; Mabry, J. M.; McKinley, G. H.; Cohen, R. E. Relationships between Water Wettability and Ice Adhesion. *ACS Appl. Mater. Interfaces* **2010**, *2*, 3100–3110.
5. Varanasi, K. K.; Deng, T.; Smith, J. D.; Hsu, M.; Bhate, N. Frost Formation and Ice Adhesion on Superhydrophobic Surfaces. *Appl. Phys. Lett.* **2010**, *97*, 234102.
6. Kulinich, S. A.; Farhadi, S.; Nose, K.; Du, X. W. Superhydrophobic Surfaces: Are They Really Ice-Repellent? *Langmuir* **2011**, *27*, 25–29.
7. Jung, S.; Dorrestijn, M.; Raps, D.; Das, A.; Megaridis, C. M.; Poulikakos, D. Are Superhydrophobic Surfaces Best for Icephobicity? *Langmuir* **2011**, *27*, 3059–3066.
8. Bahadur, V.; Mishchenko, L.; Hatton, B.; Taylor, J. A.; Aizenberg, J.; Krupenkin, T. Predictive Model for Ice Formation on Superhydrophobic Surfaces. *Langmuir* **2011**, *27*, 14143–14150.
9. Kulinich, S. A.; Farzaneh, M. How Wetting Hysteresis Influences Ice Adhesion Strength on Superhydrophobic Surfaces. *Langmuir* **2009**, *25*, 8854–8856.
10. Cao, L.; Jones, A. K.; Sikka, V. K.; Wu, J.; Gao, D. Anti-Icing Superhydrophobic Coatings. *Langmuir* **2009**, *28*, 12444–12448.
11. Tourkine, P.; Merrer, M. L.; Que're', D. Delayed Freezing on Water Repellent Materials. *Langmuir* **2009**, *25*, 7214–7216.
12. Wier, K. A.; McCarthy, T. J. Condensation on Ultrahydrophobic Surfaces and Its Effect on Droplet Mobility: Ultrahydrophobic Surfaces Are Not Always Water Repellant. *Langmuir* **2006**, *22*, 2433–2436.
13. Wong, T.-S.; Kang, S. H.; Tang, S. K. Y.; Smythe, E. J.; Hatton, B. D.; Grinthal, A.; Aizenberg, J. Bioinspired Self-Repairing Slippery Surfaces with Pressure-Stable Omniphobicity. *Nature* **2011**, *477*, 443–447.
14. Kim, P.; Epstein, A. K.; Khan, M.; Zarzar, L. D.; Lipomi, D. J.; Whitesides, G. M.; Aizenberg, J. Structural Transformation by Electrodeposition on Patterned Substrates (STEPS): A New Versatile Nanofabrication Method. *Nano Lett.* **2012**, *12*, 527–533.
15. Kim, P.; Adorno-Martinez, W. E.; Khan, M.; Aizenberg, J. Enriching Libraries of High-Aspect-Ratio Micro- or Nanostructures by Rapid, Low-Cost, Benchtop Nanofabrication. *Nat. Protoc.* **2012**, *7*, 311–327.
16. Liu, A. S.; Bezerra, M. C.; Cho, L. Y. Electrodeposition of Polypyrrole Films on Aluminum Surfaces from a *para*-Toluene Sulfonic Acid Medium. *Mater. Res.* **2009**, *12*, 503–507.
17. Paisal, R.; Martínez, R.; Padilla, J.; Romero, A. J. F. Electrosynthesis and Properties of the Polypyrrole/Dodecylbenzene Sulfonate Polymer. Influence of Structural Micellar Changes of Sodium Dodecylbenzene Sulfonate at High Concentrations. *Electrochim. Acta* **2011**, *56*, 6345–6351.
18. Stefl, B. A.; George, K. F. Antifreezes and Deicing Fluids. In *Kirk-Othmer Encyclopedia of Chemical Technology*; John Wiley & Sons, Inc.: New York, 2000.
19. Furmidge, C. G. L. Studies at Phase Interfaces I. The Sliding of Liquid Drops on Solid Surfaces and a Theory for Spray Retention. *J. Colloid Sci.* **1962**, *17*, 309–324.
20. Guo, P.; Zheng, Y.; Wen, M.; Song, C.; Lin, Y.; Jiang, L. Icephobic/Anti-Icing Properties of Micro/Nanostructured Surfaces. *Adv. Mater.* **2012**, *24*, 2642–2648.
21. Wilson, P. W.; Haymet, A. D. J. Effect of Solutes on the Heterogeneous Nucleation Temperature of Supercooled Water: An Experimental Determination. *Phys. Chem. Chem. Phys.* **2009**, *11*, 2679–2682.